Electron emission in He^+-atom and He^+-molecule collisions: A combined experimental and theoretical study

R. D. DuBois
Pacific Northwest Laboratory, Richland, Washington 99352

Steven T. Manson
Department of Physics and Astronomy, Georgia State University, Atlanta, Georgia 30303
(Received 27 December 1989)

An experimental and theoretical study of the electron emission, differential in emission angle and energy, is presented for He^+ impact on several gaseous targets. Experimentally, data at 400-, 500-, and 750-keV/amu impact on He, Ne, Ar, Kr, and H_2O are presented; theoretically, cross sections for He and Ar are calculated using the first-order Born approximation. By measuring the total electron emission, as well as electron-scattered projectile coincidences, contributions to the differential cross sections resulting from projectile ionization, from target ionization, and from simultaneous projectile-target ionization events are identified. Theoretical cross sections for each of these processes, as well as their total sum, are compared with the experimental data. From these comparisons, it is found that the present theoretical treatment does a reasonable job of describing the total projectile and target ionization cross sections, but is poor for the double-differential cross section. It also severely underestimates the simultaneous projectile-target ionization cross section.

I. INTRODUCTION

Experimental and theoretical studies of electron emission occurring as a result of collisions between charged particles and target atoms and molecules provide information about interaction mechanisms and the atomic structure of the collision partners. The experimental data, if sufficiently detailed, can be used to test our theoretical understanding of the ionization process and to evaluate where theoretical problems do, or do not, exist. Differential electron emission measurements provide this type of detailed information and test the theoretical models in much greater detail than do measurements of total ionization cross sections.

Past doubly differential studies of electron emissions resulting from fast, fully stripped ion impact on atomic targets, e.g. H^+-He and H^+-Ar collisions,[1,2] have shown that the Born approximation does a reasonably good job for fast structureless projectile impact on light targets and a slightly poorer job for heavier targets. The present work extends this type of detailed comparison to ionization occurring as a result of structured particle impact. The one-electron projectile, He^+, is studied since it is amenable to accurate theoretical treatment; He and Ar targets provide information about the accuracy of the theoretical treatment for light and heavy targets. By also experimentally studying Ne, Kr, and H_2O targets, similarities and differences for various targets can be investigated.

Ionization occurring as a result of structured particle impact is considerably more complex than ionization resulting from bare ion impact due to the presence of bound projectile electrons. These electrons affect the ionization process in two major ways, i.e., they partially screen the incoming nuclear charge and they can be excited to discrete or continuum states during the interaction. From a theoretical viewpoint, this complicates the problem since calculations must be performed for each of several ionization pathways, namely, (a) target ionization with the restriction that the projectile remains in the ground state, (b) target ionization resulting from collisions where the projectile is simultaneously excited either to discrete or continuum states, (c) projectile ionization with the target remaining in the ground state, and (d) projectile ionization with simultaneous excitation of the target. The calculations must also include the effects of dynamic screening for ionization of the target *and* for ionization of the projectile.

Experimentally, information about the screening function can be obtained by comparing electron emission spectra obtained for structured and fully stripped projectiles.[3-6] Experimental data obtained for ionization by structured projectiles have shown that the dynamic screening alters the electron emission spectrum with respect to that obtained for fully stripped ion impact in the following manner. For large secondary electron energies where small impact parameters dominate, the emitted electron spectrum is similar to that measured for the fully stripped projectile. But for small secondary electron energies where large impact parameters dominate, the screening is complete and the spectrum is similar to that recorded for a fully stripped projectile of charge Z-N, N being the number of bound projectile electrons. For intermediate secondary electron energies, the spectrum gradually changes between these two extremes.

In principle, the dynamic screening function can be obtained from the ratio of the differential cross sections measured for structured ion impact with respect to those measured for fully stripped ion impact. However, obtaining this ratio is complicated by the facts that the target

can also be ionized by the individual projectile electrons that end up in excited states [ionization pathway (b) above] and that the bound projectile electrons can also be ionized during the collision [ionization pathways (c) and (d) above]. Projectile ionization predominantly results in low-energy, isotropic emission in the projectile frame which, due to the kinematic transformation to the laboratory frame, appears as an "electron-loss peak" having a centroid energy determined by the velocity of the projectile. This peak, which is strongly forward peaked, must be isolated from the underlying target ionization continuum in order to obtain doubly differential cross sections (DDCS) for projectile ionization [pathways (c) and (d)]. Once this separation has been made, DDCS for target ionization [pathways (a) and (b)] are also obtained and the theoretical predictions can be tested. This is the goal of the present work: to obtain projectile ionization information by measuring ejected-electron-ionized projectile coincidences and to use this information to test the individual components of the theory separately.

Since the initial discovery of the electron-loss peak by Toburen and Wilson[7] and Burch *et al.*[8] for light- and heavy-ion impact, respectively, there have been many experimental and theoretical studies of ionization occurring in structured ion-atom collisions. Generally these studies have concentrated primarily on the intensity and shape of the electron-loss peak as a function of observation angle. However, in many cases doubly differential cross sections for the total electron emission have been reported.[3,4,6–15] Several years ago, we initiated our coincidence studies in order to obtain information about the individual ionization pathways [processes (a)–(d) described above]. Preliminary experimental results were reported for He^+-Ar collisions,[16] while a more detailed experimental and theoretical comparison was reported for He^+-He collisions,[17] but only for a single impact energy and emission angle. The present paper describes a more extensive study where additional targets (He, Ne, Ar, Kr, and H_2O) and impact energies (0.4, 0.5, and 0.75 Mev/amu) are experimentally investigated and the theoretical treatment has been extended to a heavier target—Ar.

II. EXPERIMENTAL PROCEDURE

The experimental apparatus used for the present study is shown schematically in Fig. 1. The basic technique consisted of passing a collimated beam of He^+ ions through a target gas cell, then charge-state-analyzing the beam and detecting the He^{2+} component with a surface-barrier detector. Electrons, created by ionization of the target or the projectile, exited the target cell through a slit. The electrons were energy analyzed and detected using a rotatable parallel-plate electron spectrometer and channel electron multiplier. The total electron emission at several laboratory emission angles (typically 20° and 30°) and energies (10–1500 eV) were measured, and, in addition, e^--He^{2+} coincidences were recorded. From these data, information about the DDCS for target and projectile ionization was extracted.

Experimental details relevant to the present measurement are as follows.

Projectile beam purity. The primary purpose of the experiment was to separate projectile and target ionization events by measuring electrons in coincidence with projectiles that have lost an electron. Standard electronics and a time-to-amplitude converter (TAC) were used to distinguish the time-correlated events (the real signals arising from projectile ionization in the target region) from any random uncorrelated events. However, of considerable concern was the elimination of any spurious time-correlated events arising from projectile ionization that occurred outside the target region coupled with target

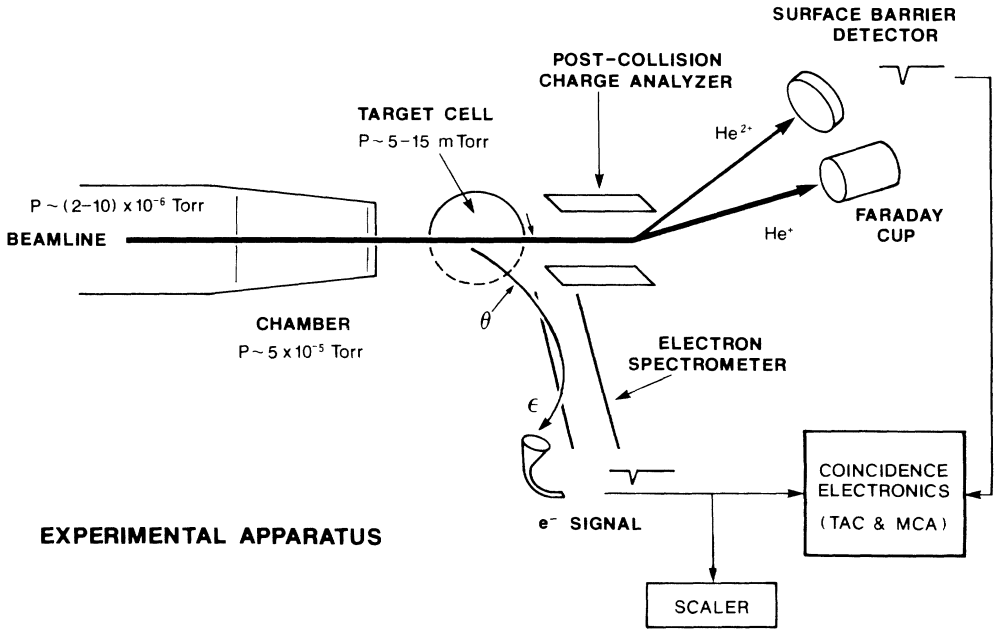

FIG. 1. Schematic of experimental apparatus showing the beam collimation system, target cell, electron spectrometer, and coincidence electronics.

ionization in the target cell. For example, the most likely possibility was that an incoming He^+ projectile might be ionized by the background gases in the beam line, thus producing a He^{2+} ion. This He^{2+} ion could then ionize the target, the net result being a time-correlated e^--He^{2+} coincidence event. But this event would *not* be due to projectile ionization resulting from collisions with the target. Likewise, an incoming He^+ ion could ionize the target and then, in a subsequent collision, be ionized itself. Again, this would produce a time-correlated coincidence signal, but not one of interest.

The second possibility—post-target stripping of the beam—was easily minimized by charge analyzing the beam immediately upon its departure from the target cell since any stripping of the beam *after* the charge-state analysis is unimportant as that stripped ion will not be deflected onto the surface-barrier detector. Tests were run with the entrance of the post-collision charge-state analyzer as close as 2.5 cm to the target cell exit and as far as 10 cm; no differences in the recorded coincidence signals were observed.

Pre-collision stripping of the beam followed by ionization of the target was minimized by making the incoming beamline as short as possible, by restricting the target gas from leaking into the beam collimator assembly, and by increasing the pumping of the beamline and the collimator assembly.

Measurements of the percentage of stripped projectile ions (typically 2–4% with target gas present and significantly less than 0.5% otherwise) compared with estimates obtained using known[18] stripping cross sections, path lengths, and pressures indicated that approximately 80–90% of the projectile ionization occurred within the target cell. This is consistent with the observed increase of the He^{2+} beam component (roughly an order of magnitude) as the target gas was added, although such an increase alone does not insure that the enhanced stripping occurred within the target cell. As a final test, coincidence cross sections measured with beamline pressures of 2×10^{-6} and 10×10^{-6} Torr showed no observable differences. Thus we are reasonably confident that the observed coincidence signals are due to projectile ionization occurring within the target cell.

Target cell. The target cell was 1.6 cm in diameter with 2-mm-diam. entrance and exit apertures. Electrons could exit from 0° to 180° through a 1-mm-wide slit in the horizontal plane. Typical target pressures, measured using a capacitance manometer, were 5 mTorr for Ar, Kr, and H_2O; 12 mTorr for Ne; and 17 mTorr for He. Test measurements using lower target pressures verified that single-collision conditions were met.

Electron detection. A rotatable (20°–150°), parallel-plate electron spectrometer (detection solid angle of ~0.002 sr and energy resolution $\Delta E/E=0.12$), and a channel electron multiplier were used to detect electrons emitted from the target cell. After correcting for the loss of electrons between the source region and the electron multiplier due to multiple scattering, the detection efficiency as a function of emitted electron energy was obtained by comparing the differential electron emission measured using the present apparatus with absolute cross sections previously reported.[1,2,4] The detection efficiency as a function of emission angle was determined from measurements of the Auger emission for H^+-Ne, Ar collisions and assuming isotropic Auger emission.

Projectile detection. The deflected He^{2+} beam component was detected by a surface-barrier detector located approximately 1 m downstream from the target region with the He^+ component being collected in a Faraday cup. An aperture 0.6 cm in diameter was placed in front of the detector to limit the possibilities for detection of unwanted scattered particles—particularly He^+ ions. The detector position (x,y) was varied to confirm that it was centered on the He^{2+} beam component and that the He^+ and He^{2+} components were well separeted. It was also demonstrated that data accumulated using the 0.6-cm aperture and the entire effective surface-barrier area, 1.2 cm in diameter, were indistinguishable. Thus, all He^{2+} ions hit the detector and unit detection efficiency for He^{2+} ions was assumed.

Background corrections. Background contributions to the measured signals originated from interactions with background gases, surfaces, or from detector "dark counts." No corrections for collisions with background gases or surfaces were made since these processes contributed primarily to an increase in the He^{2+} beam component and, as discussed above, no influence on the measured coincidence signals was observed. Using much larger beam currents and noncoincidence techniques, it was also demonstrated that background gas contributions could be neglected in the differential electron spectra. However, due to the extremely small electron counting rates for the coincidence setup (0.5–1 s^{-1} for a He^{2+} rate of $\sim130\times10^3$ counts/s), "dark counting" corrections to the total electron signal ranging from 10–70% were required. Typically the smallest electron counting rates, and hence the largest corrections, occurred for electron energies below 30 eV and above several hundred eV. For intermediate energies, dark counts contributed approximately 10–20% to the electron signal. Note that these "dark counting" corrections do not influence the coincidence signals measured for various secondary electron energies since the dark counts are randomly distributed in time. They do, however, contribute to uncertainties in the normalization procedures used to place the coincidence cross sections on an absolute scale (see below). In the coincidence channel, the TAC spectra had real to random count ratios of at least 50:1.

Absolute normalization of cross sections. Total electron emission and e^--He^{2+} coincidence data were collected as a function of electron energy for known target density and He^{2+} intensity. From these data, relative cross sections for the total electron emission and for electrons associated with projectile ionization were determined. Then the beam current was increased many orders of magnitude and absolute differential cross sections were measured in the standard fashion. The coincidence data were normalized to these absolute cross sections using the noncoincidence electron signals. The normalization was using data obtained between 30 eV and several hundred eV since, for these data, the statistical uncertainties and "dark counting" corrections were smallest. The resultant

absolute cross sections for electrons associated with projectile ionization have uncertainties resulting from the normalization procedure (approximately ±25%), limited statistics (7–12 % for the noncoincidence signals used for normalization and 8–25 % for the coincidence signals), and from background corrections that were required. Hence overall uncertainties for the coincidence cross sections associated with projectile ionization are estimated to range from ±30% for intermediate electron energies to ±40% or larger for the largest and smallest electron energies investigated. Since the target ionization cross sections were obtained via a subtraction process, they are subject to the uncertainties in both the total electron emission and coincidence signals. Hence their accuracy is difficult to quantify, particularly for conditions where projectile ionization dominates, i.e., near the electron-loss peak, where the difference between the total and coincidence signals is small. Despite these relatively large uncertainties, the present data can test our theoretical understanding of ionization occurring from He^+ impact since individual components of the calculation can be tested separately. Previously available, noncoincidence data, although having considerably smaller experimental uncertainties, can only test the sum of these components.

III. THEORETICAL TECHNIQUE

Within the framework of the first Born approximation, we consider a fast bare projectile of charge Ze, mass M, and momentum $\hbar\mathbf{k}_0$ [kinetic energy $T=(\hbar k_0)^2/2M$] ionizing a stationary target. The momentum of the electron ejected from the target is $\hbar\mathbf{k}$ and its energy in terms of the Rydberg energy is $\varepsilon/R=(ka_0)^2$, where a_0 is the Bohr radius. If the momentum of the scattered particle is $\hbar\mathbf{k}_f$, then the momentum transfer during the collision is $\hbar\mathbf{k}=\hbar\mathbf{k}_0-\hbar\mathbf{k}_f$. The *triple* differential cross section (TDCS) for ejection of an nl target electron, differential in the direction of the scattered particle ($d\Omega$), the direction of the ejected electron ($d\Omega_e$), and the energy lost by the projectile ($\varepsilon+I$, I being the ionization potential of the nl electron) is given by

$$\frac{\partial^3\sigma_{nl_0,\epsilon\mathbf{k}}}{\partial(\varepsilon/R)\partial\Omega_e\partial\Omega}=\frac{N_{nl_0}}{T/R}\frac{M/m}{\pi K^4}k_0k_f\sum_{l,l',\lambda,\lambda',L}i^{\lambda+\lambda'+l+l'}Z^2e^{i(\xi_l-\xi_{l'})}R_{nl_0,\epsilon l}(K)R_{nl_0,\epsilon l'}(K)(2L+1)$$
$$\times(2l+1)(2l'+1)(2\lambda+1)(2\lambda'+1)\begin{bmatrix}l' & \lambda' & l_0\\ 0 & 0 & 0\end{bmatrix}$$
$$\times\begin{bmatrix}l & \lambda & l_0\\ 0 & 0 & 0\end{bmatrix}\begin{bmatrix}l & l' & L\\ 0 & 0 & 0\end{bmatrix}\begin{bmatrix}\lambda & \lambda' & L\\ 0 & 0 & 0\end{bmatrix}\begin{Bmatrix}\lambda & \lambda' & L\\ l' & l & l_0\end{Bmatrix}P_L(\cos\theta_{eK})\ , \tag{1}$$

where m is the electron mass, N_{nl_0} is the number of electrons in the nl subshell, and

$$\begin{bmatrix}a & b & c\\ d & b & f\end{bmatrix}\ \text{and}\ \begin{Bmatrix}a & b & c\\ d & e & f\end{Bmatrix}$$

are the Wigner 3-j and 6-j symbols.[19] P_L is the Legendre polynomial of order L, and θ_{eK} is the angle between the ionized-electron direction k and the momentum-transfer vector K. In this formalism, all the dynamical information is contained in the ξ_l's, which are the continuum-wave phase shifts (with respect to free waves), and the ionization amplitudes,

$$R_{nl_0,\epsilon l}(K)=\int_0^\infty u_{\epsilon l}(r)j_\lambda(Kr)u_{nl_0}(r)dr\ , \tag{2}$$

with j_λ being the spherical Bessel function, and u_{nl_0} and u_{ϵ_l} the radial parts of the discrete and continuum wave functions, respectively.

To focus on the dynamical information, we rewrite Eq. (1) as

$$\frac{\partial^3\sigma_{nl_0,\epsilon\mathbf{k}}}{\partial(\varepsilon/R)\partial\Omega_e\partial\Omega}=\frac{N_{nl_0}}{T/R}\frac{M/m}{\pi K^4}k_0k_f\sum_{l,l',\lambda,\lambda',L}A(l,l',\lambda,\lambda',L)Z^2e^{i(\xi_l-\xi_{l'})}R^{\lambda}_{nl_0,\epsilon l}(K)R^{\lambda'}_{nl_0,\epsilon l'}(K)P_L(\cos\theta_{eK})\ , \tag{3}$$

where all the angular momentum algebra has been absorbed in the function A.

Integrating the TDCS over $d\Omega$ (the scattered particle solid angle) yields the double differential cross section (DDCS), i.e., the energy and angular distribution of ejected electrons as follows:

$$\frac{\partial^2\sigma_{l_0,\epsilon\mathbf{k}}}{\partial(\varepsilon/R)\partial\Omega_e}=\frac{2Z^2a_0^2}{T/R}\frac{M}{m}N_{nl_0}$$
$$\times\sum_{l,l',\lambda,\lambda',L}A(l,l',\lambda,\lambda',L)e^{i(\xi_l-\xi_{l'})}\left[\int_{K_{\min}}^{K_{\max}}Z^2P_L(\cos\theta_K)R^{\lambda}_{nl_0,\epsilon l}(K)R^{\lambda'}_{nl_0,\epsilon l'}(K)\frac{d(Ka_0)}{(Ka_0)^3}\right]P_L(\cos\theta_e)\ , \tag{4}$$

$$\cos\theta_K=\frac{K^2+k_0^2-k_f^2}{2k_0K}\ . \tag{5}$$

Here $E=\varepsilon+I$ is the energy loss. The upper and lower limits of integration are obtained by setting $\theta=0$ and π in the equation defining the momentum transfer K.

Implicit in the above triple and double differential cross sections is the use of wave functions that are antisymmetrized products of single-electron wave functions, i.e., central-field or Hartree-Fock wave functions. If more sophisticated wave functions are used, Eq. (2) is altered but the rest of the equations remain the same.

The accuracy of the wave functions used is important for the following reason. If theory and experiment disagree, there are two possible reasons (assuming experiment to be correct). Either the scattering theory is incorrect, or the wave functions used are inaccurate. Thus, accurate wave functions for the initial discrete and final continuum states of the target are essential. In general, reasonable central-field wave functions such as Hartree-Slater[20] (HS) are good enough, but in some cases Hartree-Fock (HF) are needed[21] or even correlated wave functions.[22] It is worthwhile to note that HS wave functions have been used with fairly good success for calculation of a variety of atomic properties and transitions[23] and HF wave functions are even better.[24]

To extend Eqs. (3) and (4) to the case where the incident particle is structured, i.e., where the projectile brings its own N electrons to the collision, is straightforward.[25] To begin with, it must be recognized that there are four ionization pathways, denoted (a) through (d) above, which must be individually calculated. The procedure is as follows. For target ionization with the projectile remaining in the ground state, pathway (a),

$$Z^2 \rightarrow |Z-F_{ii}(K)|^2 , \tag{6}$$

where $F_{ii}(K)$, the elastic form factor of the ground state $|i\rangle$ of the projectile, is given by

$$F_{ii}(K)=\left\langle i \left| \sum_J e^{i\mathbf{K}\cdot\mathbf{r}_J} \right| i \right\rangle , \tag{7}$$

the sum running over the N projectile electrons.

Clearly, from Eq. (7), the dynamic screening depends on the momentum transfer K and $F_{ii}(0)=N$, $F_{ii}(\infty)=0$. Thus for small energy transfer, which implies small momentum transfer (large impact parameter), Eq. (7) shows that $Z \rightarrow Z-N$, i.e., full screening. For large energy transfer, which implies large momentum transfer (small impact parameter), Z remains unmodified. Note, however, that this applies for ionization pathway (a) only.

To include projectile excitation from the ground state to state $|j\rangle$,

$$Z \rightarrow |F_{ij}(K)|^2 , \tag{8}$$

the elastic form factor that approaches zero for both small and large values of K. This is useful for individual projectile excitations but not for the sum since there are an infinite number of excitations available. However, due to the closure relation, the sum over all excited states (including integration over continuum states) is given by[26]

$$\sum_{j(\neq i)} |F_{ij}(K)|^2 = N-|F_{ii}(K)|^2+\left\langle i \left| \sum_{\substack{j,j' \\ j\neq j'}} e^{i\mathbf{k}\cdot(\mathbf{r}_j-\mathbf{r}_{j'})} \right| i \right\rangle , \tag{9}$$

where only the ground-state wave function appears. Although the sum rule is exact, it cannot be substituted into Eqs. (3) and (4) exactly because of the transformation between $\cos\theta_K$ and K. Hence Eq. (5) changes for different inelastic collisions since k_j varies with the energy loss. This means that the limits of integration in Eq. (4) vary with excitation energy. In practice, setting the limits of integration to be those relevant to the first excited state appears to be a reasonable approximation. Thus, we have an approximate method of treating ionization pathway (b).

Projectile ionization alone, and with simultaneous target excitation, processes (c) and (d) above, are handled exactly like pathways (a) and (b), but in the projectile reference frame. Thus ionization of the projectile by the target is calculated using the methodology detailed above after which the results are transformed into the laboratory reference frame according to[27]

$$\frac{\partial^2\sigma}{\partial\varepsilon_L\partial\Omega_L}=\left[\frac{\varepsilon_L}{\varepsilon_p}\right]^{1/2}\frac{\partial^2\sigma}{\partial\varepsilon_p\partial\Omega_p} , \tag{10}$$

$$\varepsilon_L=\varepsilon_p+E-2(\varepsilon_p E)^{1/2}\cos\theta_p , \tag{11a}$$

$$\cos\theta_L=\frac{\sqrt{E}-\sqrt{\varepsilon_p}\cos\theta_p}{\sqrt{\varepsilon_L}} , \tag{11b}$$

$$\phi_L=\phi_p . \tag{11c}$$

Here the subscripts L and p refer to the laboratory (target) and the projectile reference frames, respectively. The energies ε and E are the ejected electron and scaled projectile energies, respectively, where E is given by

$$E=Tm/M=\tfrac{1}{2}mV_t^2 , \tag{12}$$

T, V_t, and M being the projectile energy, velocity, and mass, respectively, and m is the electron mass. Note that in Eqs. (12), the polar angles θ_L and θ_p are defined such that the projectile velocity defines the forward direction in the lab, while in the projectile frame, the target velocity, as seen by the projectile, defines the forward direction. Using these techniques and formalisms, theoretical cross sections were determined for processes (a)–(d).

IV. RESULTS AND DISCUSSION

Representative experimental cross sections for total, projectile, and target electron emission are shown in Fig. 2. These data are for the largest projectile velocity (750 keV/amu) and smallest laboratory emission angle (20°) measured since these conditions emphasize the electron-loss peak. The data are for a light and a heavy atomic target, He and Kr, and a molecular target of atmospheric and biological interest, H_2O. In general, these data all demonstrate similar features. For example, the total electron emission (solid curve) is dominated by a large num-

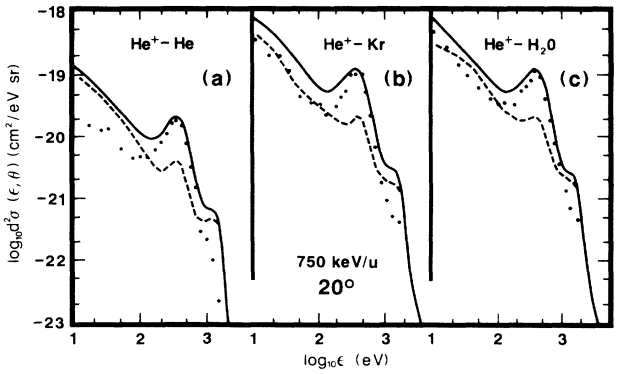

FIG. 2. Doubly differential cross sections measured for 750-keV/amu He^+ impact on He, Kr, and H_2O targets as a function of electron energy ε. The laboratory electron emission angle was 20°. ——, total electron emission; ●, electron-ionized projectile coincidences; — — —, target ionization obtained by subtraction as described in the text. Experimental uncertainties for the total electron emission are ±25% and for the e-He^{2+} coincidences, ±30–40 %. See text for details.

ber of low-energy electrons and demonstrates a broad electron-loss peak (projectile ionization) for electron energies where the electron and projectile ion velocities are equal, i.e., approximately 400 eV, and has a small hump near 1500 eV resulting from binary collisions between a target electron and the projectile. Many of these features have been discussed in detail previously (see, for example, Refs. 1–3, 7–9, and 12).

The coincidence cross sections (●) demonstrate a large peak near 400 eV due to projectile ionization, as expected. However, this peak is seen to sit on a background having features similar to those noted for the total electron emission curves. We previously[17] attributed this background to target ionization accompanied by projectile ionization, i.e., simultaneous ionization of both collision partners. This prediction has recently[28] been supported by measuring target-ion–projectile-ion coincidences for He^+–rare-gas collisions where total cross sections for simultaneous projectile-target ionization processes were found to be important contributors to the total electron emission. The present data show that these processes contribute approximately half of the total electron emission observed at 20° for low to intermediate electron energies.

Cross sections for target ionization, without any associated projectile ionization (— — —), demonstrate features similar to those previously observed for fully stripped ion impact, namely, a cross section that decreases with increasing electron energy and a binary encounter peak near 1500 eV. In addition, a peak near 400 eV is seen for all three targets. This peak is probably an artifact of the subtraction process used to obtain the target ionization cross sections since the only target ionization process that could produce a peak at that energy is electron capture to the continuum (ECC) and ECC should be negligible for the angles and impact velocities currently studied.

Thus the projectile and target ionization curves for all three targets demonstrate similar, and understandable, features. The most interesting new information suggested by the experimental data is the importance of simultaneous projectile-target ionization and how it contributes to the differential cross section.

Theoretical calculations of the DDCS for He^+-He and He^+-Ar collisions have been performed using the methodology described above. Before proceeding to a comparison of theory and experiment, some remarks regarding the physics included (and omitted) are useful in order to provide *a priori* a feeling for where the calculation is expected to be valid. Since the calculation uses the first Born approximation and uncorrelated wave functions, neither capture to the continuum nor multiple ionization processes are included. In addition, autoionizing and Auger processes are omitted. Thus, where any of these processes are of great importance, the calculation is expected to yield poor agreement with experiment.

However, autoionizing and Auger processes should be of minor importance for the impact energies considered here, as is also expected for capture to the continuum processes. In addition, data presented in Ref. 28 indicate that the predominant electron production channels are single ionization of the target, single ionization of the projectile, and simultaneous ionization of both the target and the projectile, all of which are treated by the present theory.

However, our theoretical treatment uses an approximate sum rule to obtain the cross sections for ionization of one collision partner with simultaneous excitation (which includes ionization) of the other collision partner, e.g., ionization pathways (b) and (d). By choosing the integration limits relevant to the lowest state of excitation, the calculation should provide an overestimate. Furthermore, there is some double counting in summing over the ionization pathways to obtain the total DDCS. This means that for the pathways (b) and (d) some of the simultaneous projectile-target ionization-excitation terms are identical, thus leading to an overestimation of the total DDCS. This, however, is not expected to lead to serious deviations from experiment.

As mentioned above, an accurate theoretical treatment requires good wave functions to describe the initial and final states of the system. The present calculations used central-field HS wave functions[20] except for the $3p \rightarrow d$ channel in Ar where HF discrete and continuum wave functions were employed (see Ref. 21 for details). These choices of wave functions have provided reasonably accurate descriptions for proton-impact ionization of He (Ref. 1) and Ar (Ref. 21) and are expected to yield reasonable results for He^+ impact as well. Thus, overall, the present theoretical treatment is expected to provide a reasonable description of the ionization process.

A comparison of the experimental and theoretical cross sections for 500-keV/amu He^+-He collisions is shown in Fig. 3. The laboratory observation angle is 20°. The experimental data are designated in the same fashion as was used in Fig. 2. The theoretical cross sections for target and projectile ionization are given upper and lower limits determined by the inclusion or exclusion of simultaneous excitation of the collision partner, e.g., projectile ionization is predicted to have a lower bound given by

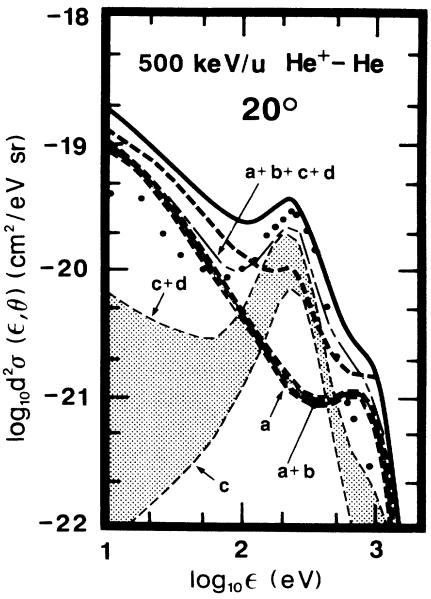

FIG. 3. Experimental and theoretical doubly differential cross sections for 500-keV/amu He^+-He collisions. The laboratory electron emission angle was 20°. The experimental data are designated as for Fig. 2. The theoretical cross sections are for target ionization (curves a, $a+b$), projectile ionization (curves c, $c+d$), and for total electron emission (curve $a+b+c+d$) where the letters indicate various ionization processes as described in the text. The shaded areas between the theoretical target and projectile ionization curves indicate that the calculations are expected to provide lower and upper bounds for these processes.

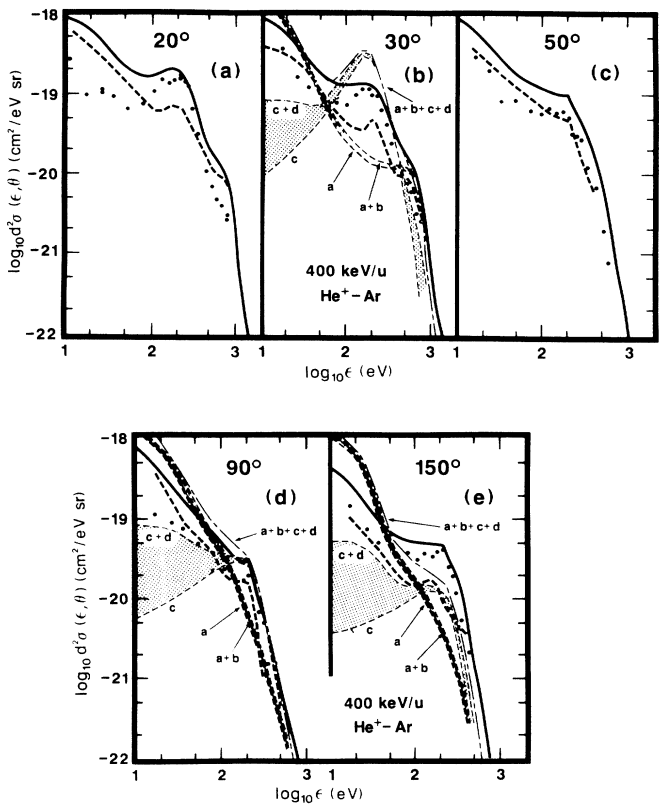

FIG. 4. Experimental and theoretical doubly differential cross sections for 400 keV/amu He^+-Ar collisions. Nomenclature is as given for Fig. 3.

curve c and an upper bound given by curve $c+d$ where the letters refer to the ionization pathways described earlier in this paper.

Overall, the comparison indicates that theory underestimates the total electron emission (experiment, ——; theory, — — —) by approximately a factor of 2 but reproduces the electron energy dependence quite well. Projectile ionization (experiment, ●; theory, curves c and $c+d$) is likewise underestimated by approximately the same amount for electron energies above 100 eV; for lower energies, the relative importance of simultaneous projectile-target ionization is severely underestimated. Target ionization (experiment, — — —; theory, curves a and $a+b$) seems to be adequately handled by theory, at least in a relative sense. The large deviation near 250 eV is attributed in part to the omission of charge transfer to the continuum in the present theoretical treatment and in part to inadequacies of the subtraction procedure used to obtain the experimental target-ionization information.

From this single comparison we would conclude that the theoretical treatment does a good job in describing target ionization and projectile ionization qualitatively but seriously underestimates the contribution of simultaneous ionization of both collision partners. This would imply that the dynamic screening is handled reasonably well but that the long-range interactions resulting in projectile ionization by the neutral target need to be treated more accurately.

Figures 4(a)–4(e) show experimental and theoretical data for a heavier target, Ar, and also provide additional angular information since for this particular system experimental data were accumulated for several angles between 20° and 150°. The experimental data exhibit features similar to those already discussed; plus they demonstrate the forward and backward peaking of the electron-loss cross section. Note that for low-electron energies the relative importance of simultaneous ionization seems to vary as a function of observation angle. This most likely is an experimental artifact resulting from the extremely low signal rates for these data and hence the large uncertainties for the low-electron energy data.

Because the experimental data are available for a large range of emission angles, comparison with theory provides some useful insights that are otherwise unavailable. From the previous comparison for He^+-He collisions, we would expect reasonable results for projectile ionization and perhaps slightly poorer results for target ionization due to the more complicated target wave functions required. However, this is not the case. Comparing the experimental and theoretical cross sections for total, target, and projectile ionization at 30°, 90°, and 150° yields poor agreement. Although the general features are reproduced, the calculated target-ionization cross sections are

too large for low-electron energies and fall off too rapidly for larger electron energies. Projectile ionization is much too large in the forward direction and decreases much too rapidly with increasing angle. In general, the theoretical cross sections do a poor job qualitatively and a very poor job quantitatively in describing the measured cross sections.

Owing to the number and kinds of approximations made in the calculations described above, there are a number of reasons for the quantitative discrepancies between experiment and theory. The overestimation of the low-energy DDCS for Ar results from a defect in the target wave functions used. This defect also appears in proton-impact DDCS (Ref. 21) and can only be cured by the use of correlated wave functions.[22] A larger discrepancy, however, is seen to be in the theoretical treatment of simultaneous ionization which is almost an order of magnitude below experiment for low-energy production, despite the fact that the calculation should be an overestimate. Clearly, correlation between projectile and target electrons, omitted in our single-particle treatment, is of great importance.

The DDCS in the region of the electron-loss peak is also not predicted well by the present theoretical treatment. It is sometimes too high and sometimes too low, as seen in Fig. 4. Since this region is dominated by projectile ionization, it follows that the present theory predicts projectile ionization poorly. Since the projectile is ionized by a neutral target atom, it may be that the absence of any long-range Coulomb field makes the results extremely sensitive to the target wave functions used.

Although the comparison between experimental and theory was not as good as we would like, it is useful to integrate the doubly differential cross sections in order to obtain total cross sections for target, projectile, and simultaneous target-projectile ionization and compare these cross sections with similar cross sections derived from projectile ion-target ion coincidence studies.[28] Experimentally, this integration could only be performed for 400-keV/amu He^+-Ar collisions because of insufficient angular information for the other systems investigated. by integrating the measured target ionization and the coincidence cross sections from 0 to 100 eV (the region containing most of the cross section) and then over angles, total cross sections were obtained. In the integration over electron energy, a constant cross section for electron energies between 0 and 10 eV was assumed. The results of the double integration were 2.1×10^{-16} cm^2 for the pure target ionization cross section and 1.1×10^{-16} cm^2 for the simultaneous projectile-target ionization cross section. These compare reasonably well with the values of approximately 3.3 and 1.4×10^{-16} cm^2 obtained from Ref. 28.

Similar integrations performed using the theoretical data yield values of 4.1 and 0.7×10^{-16} cm^2 for the target and simultaneous ionization cross sections, respectively. Clearly the agreement between experiment and theory is significantly better for these total cross sections than was found for the DDCS. This shows the value of measuring cross sections as differential as possible in order to properly assess the validity of any theoretical treatment.

V. CONCLUSIONS

Cross sections, differential in emission angle and energy, were measured for He^+ impact on several atomic targets and one molecular target. By using coincidence techniques, contributions to the total electron emission resulting from projectile ionization, from target ionization, and from simultaneous projectile-target ionization events were identified. Although the experimental uncertainties are rather large, the data demonstrate that simultaneous projectile-target ionization contributes significantly to the differential electron emission for lower emission energies. This contribution was found to be important for all targets and impact energies investigated.

Detailed calculations using the first Born approximation were made for the He and Ar targets. By comparing the calculated cross sections with the experimental results, it was shown that whereas the present theoretical treatment does a reasonably good job in predicting the total target and projectile ionization cross sections, it does a much poorer job in describing the DDCS. In particular, it severely underestimates the amount of simultaneous projectile-target ionization that was observed. Although these comparisons indicate specific needs, such as the inclusion of correlation, in future theoretical treatments, a more important message that this comparison provides is the need to compare experiment and theory in a mode as differential as possible.

ACKNOWLEDGMENTS

This work was supported by the Office of Health and Environmental Research (OHER), U.S. Department of Energy, Contract No. DE-AC06-76RL0 1830; by the National Science Foundation; and by U.S. Army Research Office Contract No. DAAL03-89-K-0098.

[1]S. T. Manson, L. H. Toburen, D. H. Madison, and N. Stolterfoht, Phys. Rev. A **12**, 60 (1975).

[2]T. L. Criswell, L. H. Toburen, and M. E. Rudd, Phys. Rev. A **16**, 508 (1977).

[3]L. H. Toburen, W. E. Wilson, and R. J. Popowich, Radiat. Res. **82**, 27 (1980).

[4]S. T. Manson and L. H. Toburen, Phys. Rev. Lett. **46**, 529 (1981).

[5]L. H. Toburen, N. Stolterfoht, P. Ziem, and D. Schneider, Phys. Rev. A **24**, 1741 (1981).

[6]J. Schader, R. Latz, M. Burkhard, H. J. Frischkorn, D. Hofmann, P. Koschar, K. O. Groeneveld, D. Berenyi, A. Kover, and Gy. Szabo, J. Phys. (Paris) Lett. **45**, L249 (1984); Nuovo Cimento **7**, 219 (1986).

[7]W. E. Wilson and L. H. Toburen, Phys. Rev. A **7**, 1535 (1973).

[8]D. Burch, H. Wieman, and B. Ingalls, Phys. Rev. Lett. **30**, 823 (1973).

[9]L. H. Toburen and W. E. Wilson, Phys. Rev. A **19**, 2214 (1979).

[10]N. Stolterfoht, D. Schneider, D. Burch, H. Wieman, and J. S. Risley, Phys. Rev. Lett. **33**, 59 (1974).
[11]M. H. Day, J. Phys. B **14**, 231 (1981).
[12]D. Schneider, M. Prost, N. Stolterfoht, G. Nolte, and R. DuBois, Phys. Rev. A **28**, 649 (1983).
[13]M. A. Bolorizadeh and M. E. Rudd, Phys. Rev. A **33**, 893 (1986).
[14]H. M. Hartley and H. R. J. Walters, J. Phys. B **20**, 3811 (1987).
[15]A. Kover, Gy. Szabo, L. Gulyas, K. Tokesi, D. Berenyi, O. Heil, and K. O. Groeneveld, J. Phys. B **21**, 323 (1988).
[16]R. D. DuBois, Nucl. Instrum. Methods B **10/11**, 120 (1985).
[17]R. D. DuBois and S. T. Manson, Phys. Rev. Lett. **57**, 1130 (1986).
[18]P. Hvelplund and E. Horsdal Pedersen, Phys. Rev. A **9**, 2434 (1974).
[19]A. Messiah, *Quantum Mechanics* (North Holland, Amsterdam, 1966), p. 1081.
[20]F. Herman and S. Skillman, *Atomic Structure Calculations* (Prentice-Hall, Englewood Cliffs, NJ, 1963).
[21]D. H. Madison and S. T. Manson, Phys. Rev. A **20**, 825 (1975).
[22]T. Burnett, S. P. Roundtree, G. Doolen, and W. D. Robb, Phys. Rev. A **13**, 626 (1976).
[23]S. T. Manson and J. E. Purcell, Phys. Rev. A **15**, 1319 (1977).
[24]M. Cohen and R. P. McEachran, Adv. At. Mol. Phys. **16**, 1 (1980).
[25]J. S. Briggs and K. Taulbjerg, *Structure and Collisions of Ions and Atoms*, edited by I. A. Sellin (Springer-Verlag, Berlin, 1978), pp. 112–117.
[26]M. Inokuti, Rev. Mod. Phys. **43**, 297 (1971).
[27]F. Drepper and J. S. Briggs, J. Phys. B **9**, 2063 (1978).
[28]R. D. DuBois, Phys. Rev. A **39**, 4440 (1989).

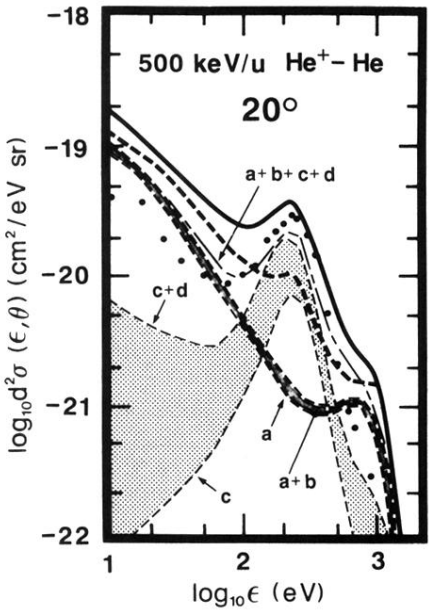

FIG. 3. Experimental and theoretical doubly differential cross sections for 500-keV/amu He^+-He collisions. The laboratory electron emission angle was 20°. The experimental data are designated as for Fig. 2. The theoretical cross sections are for target ionization (curves a, $a+b$), projectile ionization (curves c, $c+d$), and for total electron emission (curve $a+b+c+d$) where the letters indicate various ionization processes as described in the text. The shaded areas between the theoretical target and projectile ionization curves indicate that the calculations are expected to provide lower and upper bounds for these processes.

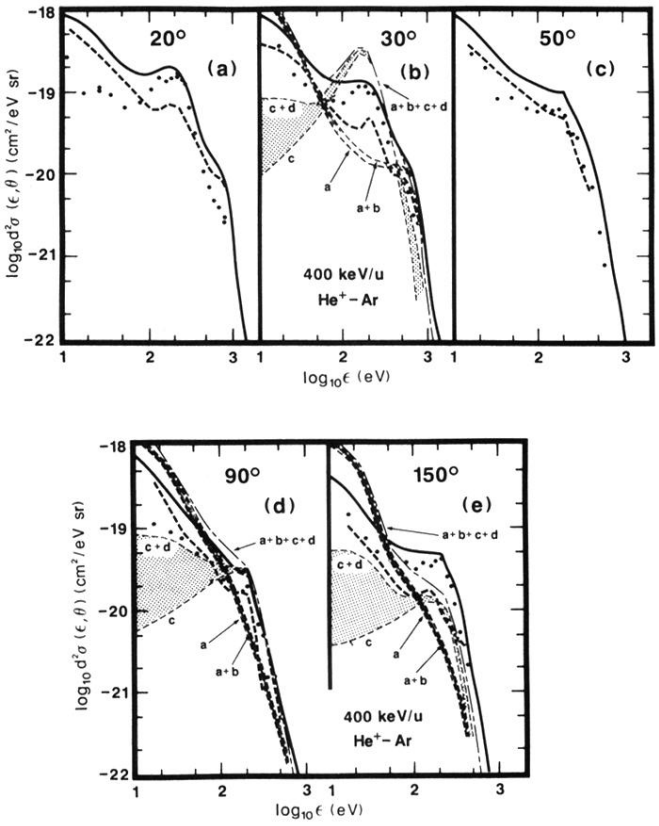

FIG. 4. Experimental and theoretical doubly differential cross sections for 400 keV/amu He^+-Ar collisions. Nomenclature is as given for Fig. 3.